Journal of Materials Chemistry

Dynamic Article Links

Cite this: J. Mater. Chem., 2012, 22, 16051

www.rsc.org/materials

PAPER

Electrochemical properties of composite fuel cell cathodes for $La_{5.5}WO_{12-\delta}$ proton conducting electrolytes†

Cecilia Solís,[a] Laura Navarrete,[a] Stefan Roitsch[b] and José M. Serra*[a]

Received 2nd April 2012, Accepted 3rd June 2012
DOI: 10.1039/c2jm32061d

New composite cathodes for proton conducting solid oxide fuel cells (PC-SOFCs) based on the novel $La_{5.5}WO_{12-\delta}$ (LWO) electrolyte have been developed. First the applicability of LWO as a protonic electrolyte has been proved by recording the OCV in a Pt/LWO/Pt cell as a function of the temperature, matching the expected Nernst voltage. In order to improve the electrode performance on LWO PC-SOFCs, composite cathodes have been prepared by mixing the $La_{0.8}Sr_{0.2}MnO_{3-\delta}$ (LSM) electronic phase with the LWO protonic phase. The ceramic–ceramic (cer–cer) composites have been electrochemically studied as cathodes on LWO dense electrolytes in symmetrical cells. Different ratios of both phases and two different electrode sintering temperatures (1050 and 1150 °C) have been studied. Electrochemical impedance spectroscopy (EIS) analysis has been carried out in the temperature range 700–900 °C under moist (2.5% H_2O) atmospheres. Different oxygen partial pressures (pO_2) have been employed in order to characterize the processes (surface reaction and charge transport) taking place at the composite cathode. A substantial improvement in the cathode performance has been attained by the addition of the LWO protonic phase into the LSM electronic material. From the electrochemical analysis it can be inferred that electrode enhancement is principally ascribed to the increase in the three-phase-boundary length, which enables electrochemical reactions to occur along the thickness of the electrode.

1. Introduction

Proton conducting solid oxide fuel cells (PC-SOFCs)[1–4] have attracted much attention nowadays due to their important advantages compared to conventional oxygen-ion conducting solid oxide fuel cells (SOFCs). In PC-SOFCs, efficiency and fuel utilization are higher since protons react with oxygen in the cathode to form water diluting the air stream. In contrast, operation in conventional SOFCs (based on oxide-ion conducting electrolytes) involves the progressive dilution of hydrogen stream with steam. Moreover, thanks to the lower activation energy of the proton transport and higher proton mobility, it is also possible to reduce the operation temperature (500–700 °C), which permits the utilization of less expensive system components and increasing their lifetime.[2,5–7] However, the use of protonic electrolytes poses a new challenge, the development of sufficiently active electrode catalysts for the corresponding partial reactions:

$$\frac{1}{2}O_2 + 2H^+ + 2e^- \rightarrow H_2O, \quad \text{in the cathode} \qquad (1)$$

$$H_2 \rightarrow 2H^+ + 2e^-, \text{ in the anode} \qquad (2)$$

Different proton conduction materials are investigated as promising electrolytes for PC-SOFCs[8–11] and, depending on the selected electrolyte material, compatible cathodes have to be developed. Recent works on PC-SOFC cathode performance have shown that the addition of a protonic conducting phase, normally the same material used as electrolyte, to a mostly electronic conducting cathode enables an important improvement of the electrochemical performance. This positive effect is ascribed to the fact that the protonic phase allows extending the three phase boundary (TPB) area from the electrode–electrolyte interface to the whole thickness of the cathode.[12–18] Furthermore, as the electrolyte material is part of the composite cathode, the electrode adhesion is improved and the thermal expansion coefficient (TEC) between the electrode and electrolyte is better adjusted and, therefore, improved mechanical properties and resistance to thermal cycling are generally attained.

Classic proton conductors based on perovskites (Sr/Ba cerates and zirconates) present high proton conductivity for application as PC-SOFC electrolytes although they typically present the following issues: (1) low sintering activity; (2) high grain boundary resistance; and (3) low chemical stability in high steam

[a]Instituto de Tecnología Química (Universidad Politécnica de Valencia – Consejo Superior de Investigaciones Científicas), Avenida de los Naranjos s/n.46022, Valencia, Spain. E-mail: jmserra@itq.upv.es; Fax: +34 963 877 809

[b]Ernst Ruska-Centre for Microscopy and Spectroscopy with Electrons, RWTH Aachen University, Ahornstr. 55, 52074 Aachen, Germany

† Electronic supplementary information (ESI) available. See DOI: 10.1039/c2jm32061d

and CO_2 environments. New studies have shown the large potential of lanthanide tungstates, generally coined as "Ln_6WO_{12}". Ln_6WO_{12} can be described as an ordered defective fluorite structure (space group $R\bar{3}$)[19] whose symmetry depends on the rare earth element: cubic or pseudo-cubic from La to Pr, *via* pseudo-tetragonal from Nd to Gd, and rhombohedral from Tb to Lu and for Y.[20,21] Particularly, $La_{5.5}WO_{12-\delta}$ (LWO in the following) is a promising proton conducting material exhibiting a unique combination of properties: (1) high protonic conductivity and very low grain boundary resistance for ionic transport;[22–24] (2) stability in harsh environments, typically in reducing CO_2 and H_2S environments above 650 °C;[25,26] and (3) electron/electron hole conduction playing a non-negligible role above 750 °C in oxidizing and reducing atmospheres, respectively.[22,33] Therefore, this material is an appealing candidate for the PC-SOFC component although limiting its application up to 850 °C, due to expected current leakages through the electrolyte thickness at higher temperatures.

The present work aims to develop active cathodes for PC-SOFCs based on LWO electrolytes. The applicability of LWO as a protonic electrolyte is studied by recording the OCV in a Pt/LWO/Pt cell as a function of the temperature. The studied cathodes comprise mixtures of two phases, *i.e.* LSM as the main electronic conducting phase and electrocatalyst, and LWO as a proton conducting phase. The electrochemical performance was optimized by studying the effect of the LSM–LWO ratio and sintering temperature, while an electrochemical test was carried out using LWO-based symmetric cells by means of impedance spectroscopy.

2. Experimental

$La_{5.5}WO_{12-\delta}$ used for the cathodes was prepared following a citrate-complexation route. This specific stoichiometry was selected to achieve phase-pure materials, since nominal La_6WO_{12} has been shown to segregate La_2O_3.[27] La_2O_3 (Aldrich, 99.9%, pre-dried at 1100 °C) was dissolved in concentrated hot nitric acid (65% vol.) and then citric acid was added as a complexing agent.[21] Another solution was prepared using ammonium tungstate (Fluka, >99%) also with citric acid (Fluka, 99.5%). Both solutions were heated at 120 °C for 1 h. Then ammonia was added to neutralize the solutions after which they were mixed at room temperature. This solution was gradually concentrated by stepwise heating under stirring, which led to gel foaming. The product was calcined in air at 800 °C to oxidize carbonaceous matter and promote crystallization of the oxide. The desired particle size for the cer–cer fabrication was obtained after calcining the powder at 1300 °C for 10 h.

$La_{0.8}Sr_{0.2}MnO_3$ (LSM) powder was purchased from Fuel Cell Materials. It was calcined at 1000 °C for 5 h and ball-milled for 10 h in acetone in order to obtain grain sizes similar to those of LWO powder. The studied cer–cer compositions were prepared by mixing the corresponding amounts of the different powders, milling them together on an agate mortar and finally inks for screen printing were prepared by using terpineol and ethylcellulose in a roller mixer.

The crystalline phase was characterized by X-ray diffraction (XRD) using a PANalytical X'Pert PRO diffractometer, and employing CuK$\alpha_{1,2}$ radiation and an X'Celerator detector in Bragg–Brentano geometry. XRD patterns were recorded in the 2θ range from 0° to 90° and analyzed using X'Pert Highscore Plus software.

LWO Cerpotech commercial powder was used to prepare the electrolytes. LWO dense electrolytes (~1 mm thick) were obtained by uniaxally pressing the ball-milled LWO powder at ~120 MPa and final firing at 1450 °C for 5 h. Porous ~30 μm electrodes were obtained by screen-printing the inks on both sides of the LWO electrolytes. The firing temperature of the screen-printed cathode cells was 1050 °C and/or 1150 °C for 2 h. The final size of symmetrical cells was 15.5 mm in diameter whereas cathodes were ~9 mm in diameter.

Symmetrical cells were tested by electrochemical impedance spectroscopy (EIS) in a two-point configuration with platinum current collector meshes. The input signal was 0 V DC–20 mV AC in the 0.03–1 × 10^6 Hz frequency range (Solartron 1470E and a 1455A FRA module equipment). EIS measurements near OCV were performed in the 650–900 °C range, under wet atmospheres (2.5% vol. H_2O) at different pO_2 (mainly 100, 50 and 5% air) while total flow remained constant (100 mL·min^{-1}). The contribution of the LWO electrolyte has been corrected from impedance spectra. Pt/LWO/Pt (Pt porous layer was applied by screen printing) cell testing was done from 700 to 900 °C using humidified air (150 mL min^{-1}) at the cathode side and hydrogen (150 mL min^{-1}) as fuel at the anode side. Sealing was achieved using gold gaskets.

Graphite sputtered symmetrical cell cross-sections were analyzed by scanning electron microscopy (SEM) using a JEOL JSM6300 electron microscope. The microstructure of the sintered samples was characterized by means of a transmission electron microscope (TEM) FEI Tecnai F20 (with an acceleration voltage of 200 kV), equipped with an EDAX energy dispersive X-ray spectrometer. TEM lamellas were prepared by means of a FIB (Focused-Ion Beam, FEI Helios Nanolab 400s) and subsequently thinned by standard argon-ion milling techniques.

3. Results and discussion

3.1. Assessment of the electrolyte use

As a first step and with the aim to evaluate the use of the LWO protonic conductor as an electrolyte for PC-SOFCs, a Pt/LWO/Pt cell was measured as a complete cell by using hydrogen and humidified air in anode and cathode sides, respectively. The electrolyte thickness was 1 mm and the Pt electrodes were 15 μm thick and 9 mm in diameter. The measured open circuit voltage (OCV) is close to the theoretical Nernst voltage as can be observed in Fig. 1a, where the OCV is represented as a function of the temperature. From these OCV values it can be inferred that the LWO electrolyte subjected to this chemical gradient (wet air||wet H_2) behaves as a prevailing ionic conductor and the presence of leakage currents through the electrolyte ascribed to electronic conductivity is negligible. This result suggests that there must exist a certain inner electrolyte region, with minor electronic conductivity, sandwiched between two p/n-type conducting regions exposed to air and wet hydrogen, respectively. The thickness of this electrolytic region would depend on the oxygen activity (a_{O_2}) profile across the LWO *pellet*, since the

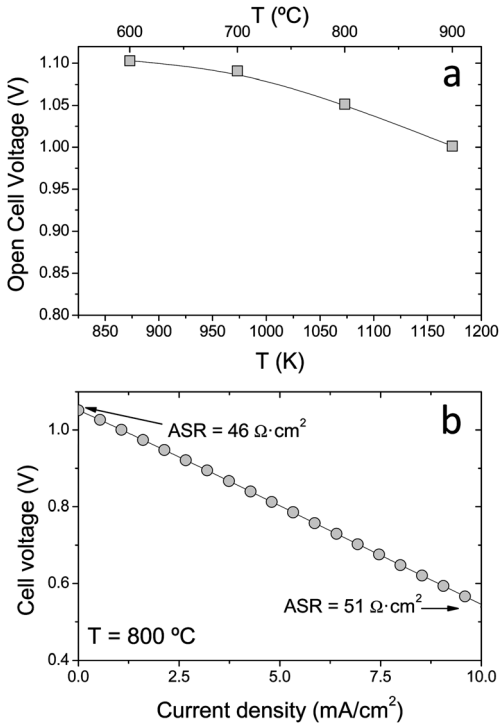

Fig. 1 OCV as a function of the temperature of a measured Pt/LWO/Pt cell (a) and cell voltage as a function of the current intensity as measured at 800 °C (b).

relationship between partial electronic conductivity and a_{O_2} (or pO_2) is well-established[22,23] and thickness independent. As a consequence, the appropriateness of LWO for its use as a protonic electrolyte can be confirmed. In Fig. 1b, the cell voltage has been plotted as a function of the current intensity at 800 °C. Despite the fact that a thick electrolyte was used and therefore the cell specific resistance is mostly determined by the electrolyte, it is remarkable that the area specific resistance (ASR) at OCV is still lower than that observed at higher current densities (lower cell voltages). This has been observed for high-temperature proton conductor-based cells employing both thick electrolytes[17] and thin supported electrolytes[28,29] and this behavior is in contrast with the inverse behavior widely reported for conventional (oxide-ion based) SOFC electrolytes.[30,31] This fact is not clearly understood although this may be related to two possible effects: (1) the activation of surface species through an imposed current/DC bias, which typically affects conventional SOFC cathodes while the nature of the partial electrode reactions is different for both types of SOFCs, and (2) the drop in the *local* concentration of hydrogen in the anode through the dilution with the formed water in conventional SOFC cells which causes a slight decrease in the cell voltage (Nernst potential) whereas this effect does not take place in the PC-SOFC anode.

3.2. Microstructural analysis of cer–cer cathodes

Once the suitable electrochemical behavior of the LWO as an electrolyte is confirmed, this work focuses on the study of LSM–LWO composite electrodes prepared by physically mixing different amounts of each phase. Firstly, the chemical compatibility of both materials has been checked by means of XRD upon heat treatment. Fig. 2 shows XRD measurements at room temperature of LSM–LWO 50 vol.% calcined at 1150 °C for 5 h. XRD patterns of single LWO (sintered at 1300 °C) and LSM (sintered at 900 °C) are also displayed for comparison. The compatibility is proved as all the peaks of the composite cathode, before and after heat treatment, can be completely assigned to both LWO and LSM phases, *i.e.*, no new diffraction peaks appeared upon treatment. Furthermore, no changes in cell parameters are observed.

As the microstructure of the cathodes constitutes a key factor for the correct fuel cell performance, the sintering temperature has been varied in order to analyze resulting differences. Fig. 3 presents the SEM micrographs corresponding to both LSM and LWO powders (left-hand) and LSM–LWO cer–cer cathodes 60/40 vol.% and 50/50 vol.% sintered at 1050 and 1150 °C (center and right-hand). Both LSM and LWO powders present similar microstructures suitable for mixing them. From the cer–cer images, the high density of the electrolyte (beneath the porous cathode) can be confirmed, presenting scarcely close porosity, while the electrode porosity is enough for gas exchange. No significant differences in the cathodes microstructure were observed between both sintering temperatures.

TEM images of the cross-section of a LSM cathode sintered at 1150 °C on LWO are shown in Fig. 4 in combination with three EDX spectra acquired in different sample regions. On the left-hand side a part of the FIB-lamella, showing the interface between LWO and LSM, is visible. In this image, the slightly bent interface is vertical. LWO is on the left-hand side and LSM on the right-hand side. A selected region is shown with higher magnification on the right-hand side of Fig. 4. Dashed lines indicate particles at the LWO–LSM interface which exhibit a variation in the stoichiometry. EDX spectra have been taken at three different positions and are indicated by numbers. Spectrum 1 has been taken on the LWO side, spectrum 3 on the LSM side, and spectrum 2 on one of the particles in between. EDX spectrum 2, however, shows that these particles mainly consist of LWO, as only a small amount of Mn (2–3 at.%) but no Sr is found. Some Mn cations might have diffused into the first grain layers of LWO. Nevertheless, this small amount of Mn may stem from measuring inaccuracy or scattered radiation from the LSM. Copper signals indicated within the EDX spectra are due to the sample holder and the casing of the microscope. In summary, TEM analysis suggests good compatibility and adhesion between

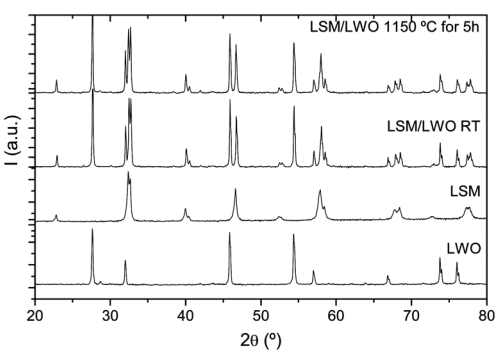

Fig. 2 XRD pattern of LWO, LSM and a LWO–LSM mixture (50 vol.%) after being treated at 1150 °C for 5 h.

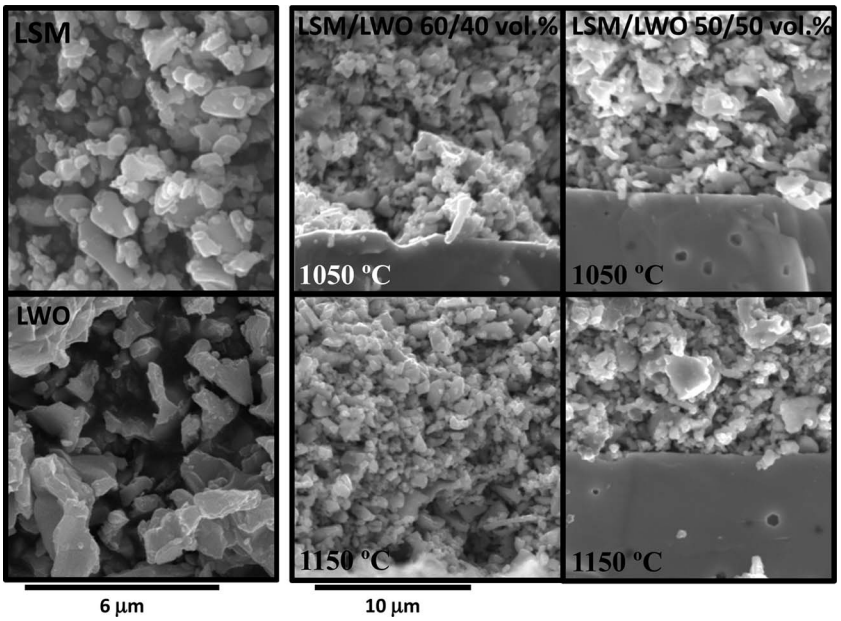

Fig. 3 SEM images of LSM and LWO powders (left-hand side) and LSM–LWO cer–cer cathodes 60/40 vol.% (center) and 50/50 vol.% (right-hand side) sintered at 1050 °C (up) and 1150 °C (down).

the LWO electrolyte and LSM porous electrode upon sintering at 1150 °C in air.

3.3. Electrochemical analysis of cer–cer cathodes

Electrochemical properties of the different ratios of LSM and LWO have been studied and compared with the reference LSM electrode. Fig. 5a shows the polarization resistances (R_p) recorded in wet (2.5% H_2O) air for different cathodes as a function of temperature in an Arrhenius arrangement. In all cases the activation energy (E_a) is close to that of other LSM reported electrodes.[32] Furthermore, Fig. 5b displays R_p at 750 °C (triangles) and 900 °C (squares) as a function of the amount of LWO added to the LSM electronic phase. From this graph it can be ascertained that the addition of up to 50 vol.% of LWO protonic phase allows decrease of R_p. The best performance is achieved for the cathode with 40 vol.% of LWO protonic phase, which behaves 5 times better than the LSM electrode. The introduction of proton-transport pathways in the cathode seems to enlarge the active electrocatalytic area in a certain electrode thickness, as previously reported for other protonic cathode composites.[16,33]

On the other hand, when the addition of the protonic phase is higher than 50 vol.% (LSM–LWO 40/60 vol.%) R_p is even worsened with regard to the LSM electrode. This drop in the cathode electrochemical performance has been attributed for other cer–cer protonic cathodes to: (i) a restriction in the active electrode thickness due to the limited protonic conductivity of LWO particles; (ii) the lower TPB length of this composition compared to that of the optimum LSM–LWO ratio; and (iii) a possible limitation of the electronic conductivity, due to the lack of sufficient connectivity among LSM particles.[18] Subsequent limitations ascribed mainly to the drop in TPB length, intra-particle conductivity and the complexity of the cathode reaction in protonic regime could be reflected in an electrochemical performance decay, as it has been assumed that percolation threshold may not be achieved at 40 vol.% of LSM (percolation threshold for LSM lies typically around 30 vol.% for conventional composite SOFC electrodes).[34,35]

In Fig. 5a two different sintering temperatures, 1050 and 1150 °C, for the 50 vol.% composite cathode can also be compared. The highest sintering temperature shows better cathode performance as it corresponds to the material with better connectivity among the particles while the surface area remains approximately the same (as observed by SEM). Consequently, the best performance is observed in the LSM–LWO 60/40 vol.% sintered at 1150 °C and therefore the rest of the cathode compositions were sintered at 1150 °C.

Impedance spectra (Nyquist and Bode plots‡) recorded at 750 °C and 900 °C in wet air and at 900 °C in 5% air diluted with N_2 for the three composite cathodes sintered at 1150 °C and the LSM–LWO 50 vol.% and the LSM cathodes sintered at 1050 °C are represented in Fig. 6. From these graphs at least two different contributions (two separated arcs) can be distinguished. One corresponds to the low frequency (LF) range, below 0.1–2 Hz, and the other one, which appears principally in the composite cathodes in the medium-to-high frequency (referred here as HF) range, around 1–10 kHz.

At 900 and 750 °C, all electrodes seem to be principally limited by LF surface-associated processes as inferred from the higher magnitude of this arc, although HF arc contribution reaches similar values with the highest amount of LWO protonic phase introduced. At 750 °C the frequency range of each contribution shifts down to lower values as it corresponds to the decrease of temperature.

It has to be emphasized that the LSM electrode is limited by LF processes and nearly no HF contribution is observed at some

‡ Note that in the impedance figures presented in this paper the left-handed graph (Nyquist) frequency evolution is increasing from left to right opposite to the right-handed graphs (Bode).

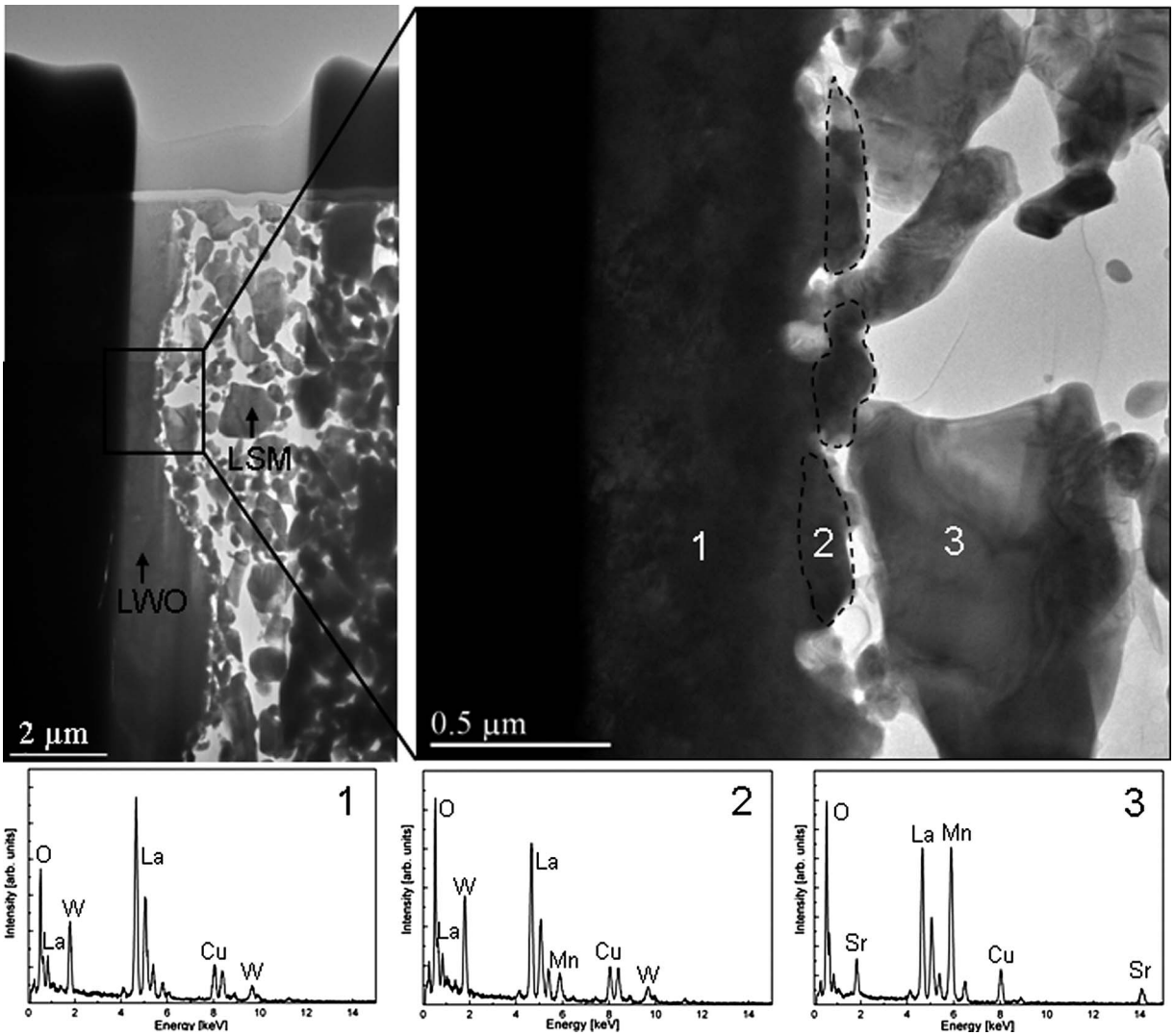

Fig. 4 TEM images and EDX spectra of a FIB-lamella showing the cross-section of a LSM cathode on the LWO electrolyte calcined at 1150 °C.

temperatures. This fact is associated to the lower TPB available for surface reactions. When the protonic phase is introduced, the LF arc decreases as a consequence of the higher available TPB extended into a certain thickness of the cathode and thanks to the newly introduced protonic pathways. However, as mentioned, the introduction of this protonic phase gives rise to the occurrence of the HF arc which increases with the amount of LWO introduced. The nature of HF processes will be discussed below.

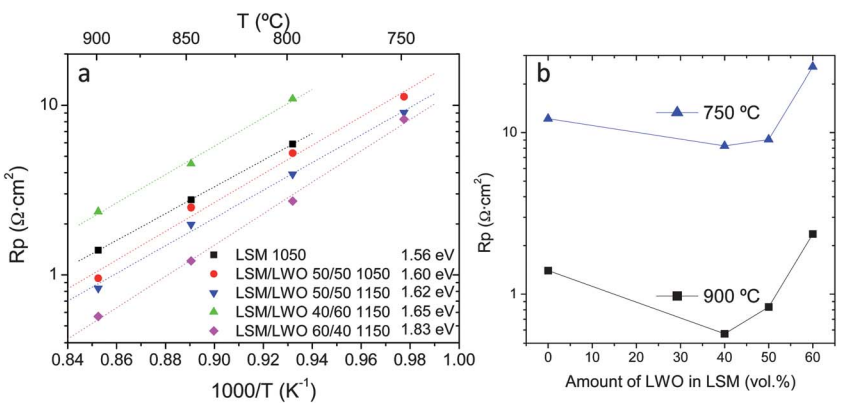

Fig. 5 R_p as a function of temperature of LSM and different cer–cer cathodes of LSM–LWO (a) and R_p at 750 °C and 900 °C as a function of the amount of LWO added to the LSM electronic phase (b).

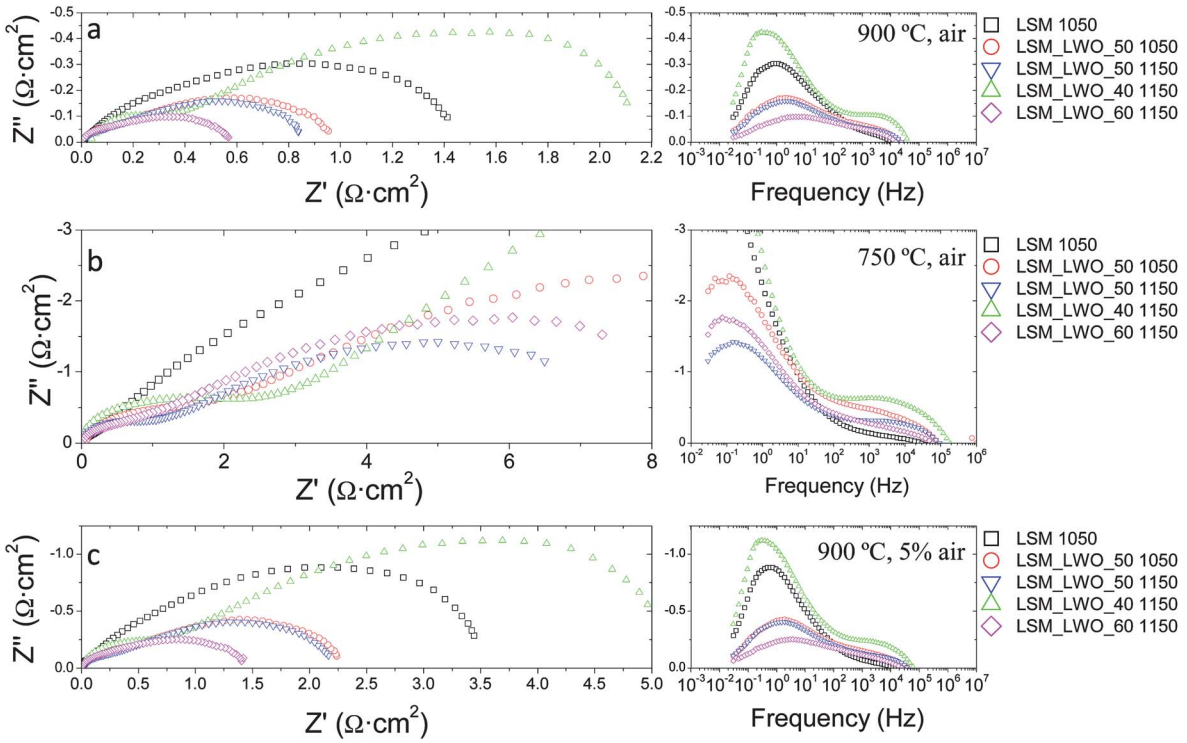

Fig. 6 Electrochemical impedance spectra (Nyquist and Bode plots‡) recorded in wet air at 900 °C (a) and 750 °C (b) and in 5% air at 900 °C (c) for LSM sintered at 1050 °C and the three composite electrodes (50/50 vol.% sintered at 1050 and 1150 °C, and the other at 1150 °C).

When pO_2 is reduced (see results in 5% air, Fig. 6 bottom), the cathode performance worsens while the LF resistance increases remarkably with regard to HF resistance. This confirms that the limiting LF processes are related to surface processes, *i.e.*, adsorption and dissociation of oxygen molecules on the surface of the electrode.

The best performing electrode based on LSM–LWO 60/40 vol.% exhibits the lowest LF processes contribution. In fact, LF resistance values of this cathode composition are similar to those for HF associated processes. Thus, the limiting steps seem to be related to surface processes and ionic transport. This composite cathode, together with the pure LSM cathode, will be analyzed in detail by means of circuit modeling of impedance spectra in the next section.

3.4. Circuit modeling results: cathode performance analysis

The recorded impedance spectra can be analyzed in terms of two (or even three in some cases) depressed arcs more or less overlapped following equivalent circuit models presented in Fig. 7, as previously anticipated. Fig. S2† shows two different examples of fittings to both equivalent circuits. In this section, the different parameters extracted from equivalent circuit modeling of the composite LSM–LWO 60/40 vol.% cathode (fitted to two arcs, Fig. 7a) and single LSM cathode (fitted to three different arcs, Fig. 7b) are analyzed as a function of temperature (Fig. 8) and pO_2 (Fig. 9). The aim of this analysis is to identify and gain insight into the possible conduction mechanisms and electrochemical processes occurring at the cathode affecting the polarization resistance and to clarify the role of each phase in the cathode performance.

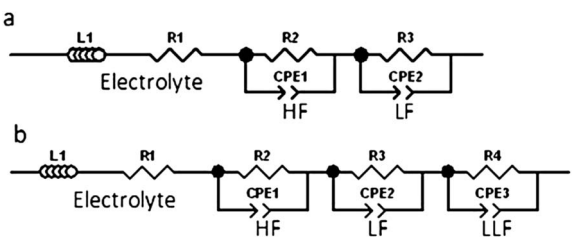

Fig. 7 Equivalent circuit models employed in the impedance data analysis.

Fig. 8 presents the obtained circuit parameters, *i.e.*, (a) the modeled resistances (R); (b) the pseudo-capacitances (C) calculated from the constant-phase-elements (CPEs);[36] and (c) relaxation times (τ) corresponding to LSM (top) and LSM–LWO 60/40 vol.% (bottom) cathodes. The most evident difference between both cathodes is that while three depressed arcs are needed for the correct fitting of the LSM cathode only two arcs are needed for the composite cathode. The extra arc of the LSM cathode appears at relatively lower frequencies ($\tau = 1$ s $\rightarrow f = 1$ Hz), and it has been labeled as LLF. The other two arcs have been marked as LF and HF (1–10 Hz and 10 kHz, respectively).

Although there are significant dissimilarities between LSM and the composite cathode, the highest R values are found for LF processes in both electrodes with associated capacitances ranging from 0.01 to 0.1 F cm^{-2}. Similar resistances and capacitances have been observed in other composite cathodes for conventional SOFCs and they have been assigned to adsorption and dissociation of oxygen molecules on the surface of the electrode.[37]

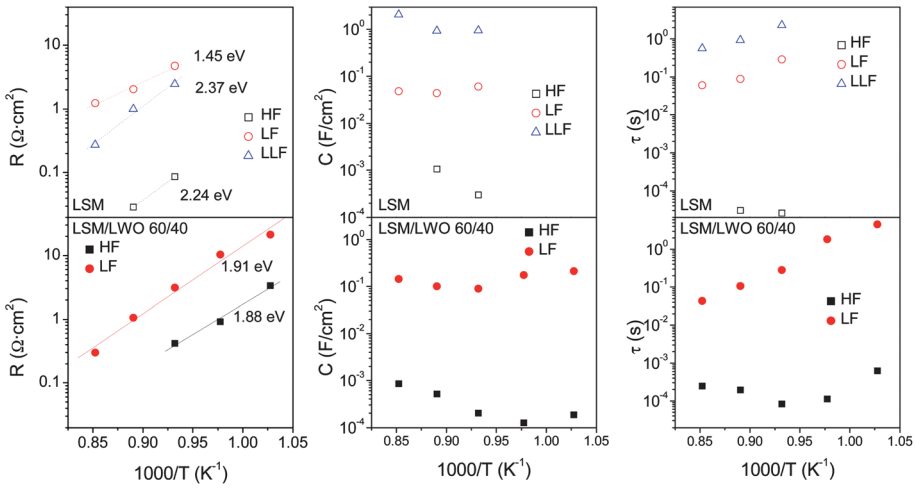

Fig. 8 High and low frequency R (a), C (b) and τ (c) obtained from the equivalent circuits of the LSM–LWO 60/40 vol.% and LSM cathodes sintered at 1150 °C measured in wet air as a function of inverse temperature.

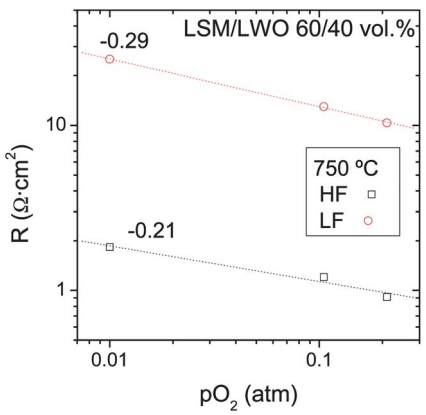

Fig. 9 LSM–LWO 60/40 vol.% cathode resistance of the HF and LF associated processes as a function of pO_2 measured at 750 °C in wet atmospheres.

In the case of LSM cathode, LLF resistance values are very close to those of LF processes and they present very high associated capacitances and activation energies (2.37 eV). These LLF processes, also limiting the performance of this LSM cathode, may be associated to the lack of protonic conductivity that highly limits the TPB area in this cathode. Namely, TPB is confined to the pores close to the cathode–electrolyte interface. The contribution of the HF processes in this case is minor compared to the limiting LF and LLF processes.

The LSM–LWO 60/40 vol.% composite cathode presents no LLF arc and this is ascribed to the introduction of the protonic network that may enable the extension of the TPB area into a certain thickness of the cathode. However, in this electrode, as the LF contribution is drastically reduced, the HF associated processes contribution is significant, or at least comparable to the LF contribution. These HF related processes can be assigned to the total transport through the cathode and also to the electrolyte–electrode interface resistance (against proton transport) that increases with the amount of protonic phase introduced, *i.e.*, the enlargement of the surface contact between both materials (LWO–LSM).

It has been broadly reported that in PC-SOFCs there exist mainly three different elementary cathode reaction steps: (1) surface dissociative adsorption and diffusion of oxygen along with charge transfer; (2) proton migration from electrolyte to TPBs; and (3) formation and desorption of H_2O.[38,39] Note that steps (2) and (3) differ from elementary reactions of common SOFCs based on oxide-ion conductor electrolytes. Thus the analysis of the resistance dependence on pO_2 and pH_2O constitutes a useful guide to explore the rate limiting steps for protonic cathode reactions as the polarization resistance (R_i) of any elementary step can be expressed as eqn (3).

$$R_i \propto pO_2^{-m_i} \cdot pH_2O^{-n_i} \quad (3)$$

If we just take into account the pO_2 dependence and keep pH_2O constant we can consider eqn (4) instead

$$R_i \propto pO_2^{-m_i} \quad (4)$$

and m gives information about the type of the species involved in the electrode reaction. Fig. 9 shows HF and LF resistance of the LSM–LWO 60/40 vol.% cathode as a function of pO_2 measured at 750 °C in wet (2.5% H_2O) atmospheres. The −0.29 power dependence of the R_{LF} (close to −3/8) together with the associated capacitances (of around 10^{-1} F cm^{-2}) and frequency range (0.2–20 Hz) have been previously reported in other composite cathodes and principally assigned to different elementary reactions in the surface dissociative adsorption and diffusion of oxygen step[38,39] $O_{ad} + e^- \rightarrow O^-_{ad}$, $m = 3/8$.

The −0.21 power dependence of the R_{HF} (close to −1/4) and the associated capacitances (10^{-3} to 10^{-4} F cm^{-2}, as can be observed in Fig. 8) can be assigned to the charge transport processes of O^-_{ad} species along the surface of the LSM phase (see diagram of Fig. 10), $O^-_{ad} \rightarrow O^-_{TPB}$, $m = 1/4$, and ionic transport from TPB interface towards the electrolyte.[39] Furthermore, this pO_2 power variation of −1/4 can be also related to the variation of the p-type electronic carriers with the pO_2 and its influence on the surface processes (as the associated frequencies are high but not so high to be related to changes in the bulk p-type electronic conductivity of the cathode).[40] Thus, this p-type electronic conductivity variation has to be associated to the surface of

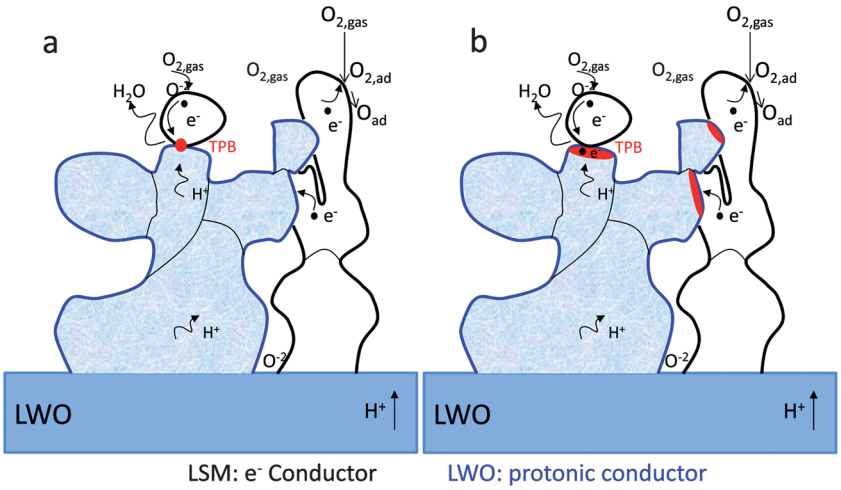

Fig. 10 Diagram of the LSM–LWO cer–cer cathode with the TPB in the point of contact of the LSM and LWO phase (a) and higher TPB area when the LWO phase presents surface electronic conductivity (b).

LWO grains[22,23] (LSM is not limiting the electronic conductivity) and could induce an increase of the available TPB area, as TPB points located in the contact points between the LSM and the LWO phases could be extended to a certain surface area on the LWO grains (see diagram of Fig. 10b).

The absence of pH_2O dependency of both LF and HF processes, observed by the same R_p obtained when measuring in both normal and heavy water (Fig. S1†), confirms the proposed reaction mechanisms. Furthermore, from the observed reaction processes it can be concluded that oxygen diffusion and transport represent the limiting mechanisms in these cathodes, being independent of the proton related processes, although protons are major charge carriers in the LWO electrolyte under these operating conditions.[22,23]

4. Conclusions

The $La_{5.5}WO_{12-\delta}$ material presents the necessary properties to consider it as a promising candidate for PC-SOFCs, *i.e.*, (1) as an electrolyte, high conductivity and predominant proton transport under H_2||air gradient, and (2) as a cathode component, good compatibility with LSM and certain p-type conductivity, along with high chemical stability. In this study, and after directly proving the feasibility of the use of LWO as a protonic electrolyte, different cer–cer composites based on LSM and LWO have been studied and analyzed as cathodes for LWO PC-SOFCs. After a thorough electrochemical characterization the improvement of the cathode performance with the addition of the LWO protonic phase to the simple LSM electrode has been proved. When the amount of LWO was 40 vol.%, the polarization resistance was halved with respect to LSM for the whole temperature range. Moreover, the resistances derived from the limiting LF and LLF processes associated with surface and TPB area were reduced, and even removed in the case of LLF, through the addition of the LWO protonic phase to the LSM cathode. This fact is ascribed to the increase in the TPB area into a certain cathode thickness with the introduction of the LWO protonic pathways. HF processes were ascribed to oxygen related charge transfer reactions. Thus, all the observed reactions, related to oxygen diffusion and transport, represent the limiting mechanisms in these cathodes, not limited by proton related processes.

Acknowledgements

Funding from European Union (FP7 Project EFFIPRO - Grant Agreement 227560), the Spanish Government (ENE2011-24761 and CSIC Intramural 200880I093 grants) is kindly acknowledged. The authors thank Dr M. Ivanova and Dr D. Sebold (Forschungszentrum Jülich, IEK-1) for sample preparation for microscopy analysis, and Mrs M. Fabuel and Dr V. B. Vert for assistance in electrochemical tests.

Notes and references

1 N. Bonanos, *Solid State Ionics*, 1995, **79**, 161.
2 H. Iwahara, T. Esaka, H. Uchida and N. Maeda, *Solid State Ionics*, 1981, **3–4**, 359.
3 T. Norby and Y. Larring, *Solid State Ionics*, 1995, **77**, 147.
4 K. D. Kreuer, *Annu. Rev. Mater. Res.*, 2003, **33**, 333.
5 N. Bonanos, *Solid State Ionics*, 1992, **53–56**, 967.
6 H. Iwahara, *Solid State Ionics*, 1995, **77**, 289.
7 N. Bonanos, K. S. Knight and B. Ellis, *Solid State Ionics*, 1995, **79**, 161.
8 R. Haugsrud and T. Norby, *Nat. Mater.*, 2006, **5**, 193.
9 P. Babilo and S. M. Haile, *J. Am. Ceram. Soc.*, 2005, **88**, 2362.
10 J. M. Serra and W. A. Meulenberg, *J. Am. Ceram. Soc.*, 2007, **90**, 2082.
11 J. M. Serra, O. Büchler, W. A. Meulenberg and H. P. Buchkremer, *J. Electrochem. Soc.*, 2007, **154**, B334.
12 E. Perry Murray and S. A. Barnett, *Solid State Ionics*, 2001, **143**, 265.
13 A. Mai, V. A. C. Haanappel, S. Uhlenbruck, F. Tietz and D. Stöver, *Solid State Ionics*, 2005, **176**, 1341.
14 C. Huang, D. Chen, Y. Lin, R. Ran and Z. Shao, *J. Power Sources*, 2010, **195**, 5176.
15 F. He, T. Wu, R. Peng and C. Xia, *J. Power Sources*, 2009, **194**, 263.
16 V. B. Vert, C. Solís and J. M. Serra, *Fuel Cells*, 2011, **11**, 81.
17 E. Fabbri, S. Licoccia, E. Traversa and E. D. Wachsman, *Fuel Cells*, 2009, **9**, 128.
18 C. Solís, V. B. Vert, M. Fabuel and J. M. Serra, *J. Power Sources*, 2011, **196**, 9220.
19 S. P. Ray and D. E. Coix, *J. Solid State Chem.*, 1975, **15**, 333.
20 G. J. McCarthy, R. D. Fisher, G. G. Johnson, Jr and C. E. Gooden, in Solid State Chemistry, *Proceedings of the 5th Materials Research Symposium*, National Bureau of Standards, Special Publication, 1972, p. 397.

21 S. Escolastico, V. B. Vert and J. M. Serra, *Chem. Mater.*, 2009, **21**, 3079.
22 R. Haugsrud and C. Kjølseth, *J. Phys. Chem. Solids*, 2008, **69**, 1758.
23 C. Solís, S. Escolastico, R. Haugsrud and J. M. Serra, *J. Phys. Chem. C*, 2011, **115**, 11124.
24 A. Magraso, J. M. Polfus, C. Frontera, J. Canales-Vazquez, L. Kalland, C. H. Hervoches, S. Erdal, R. Hancke, S. S. Islam, T. Norby and R. Haugsrud, *J. Mater. Chem.*, 2012, **22**, 1762.
25 J. M. Serra, S. Escolastico, M. Balaguer, W. A. Meulenberg, H. P. Buchkremer, T. Scherb, G. Schumacher, M. W. Lumey and R. Dronskowski, Ceramic Hydrogen-Permeable Membranes made of Mixed Proton-electronic Conducting Materials Based on the System Ln_6WO_{12}, *Proceedings of 2009 E-MRS Fall Meeting, September 14–18, Warsaw*, 2009, p. 140.
26 S. Escolástico, C. Solís and J. M. Serra, *Int. J. Hydrogen Energy*, 2011, **36**, 11946.
27 A. Magraso, C. Frontera, D. Marrero-Lopez and P. Nunez, *Dalton Trans.*, 2009, 10273.
28 N. Ito, M. Iijima, K. Kimura and S. Iguchi, *J. Power Sources*, 2005, **152**, 200.
29 E. Fabbri, L. Bi, D. Pergolesi and E. Traversa, *Energy Environ. Sci.*, 2011, **4**, 4984.
30 J. M. Serra and V. B. Vert, *ChemSusChem*, 2009, **2**, 957.
31 J. M. Serra and V. B. Vert, *J. Electrochem. Soc.*, 2010, **157**, B1349.
32 Y. Takeda, R. Kanno, M. Noda, Y. Tomida and O. Yamamoto, *J. Electrochem. Soc.*, 1987, **134**, 2656.
33 K. V. Kravchyk, E. Quarez, C. Solís, J. M. Serra and O. Joubert, *Int. J. Hydrogen Energy*, 2011, **36**, 13059.
34 D. Chen, L. Lu, J. Li, Z. Yu, W. Kong and H. Zhu, *J. Power Sources*, 2011, **196**, 3178.
35 C. Nicolella, A. Bertei, M. Viviani and A. Barbucci, *J. Appl. Electrochem.*, 2009, **39**, 503.
36 S. M. Haile, D. L. West and J. Campbell, *J. Mater. Res.*, 1998, **13**, 1576.
37 M. J. Jørgensen and M. Mogensen, *J. Electrochem. Soc.*, 2001, **148**, A433.
38 F. He, T. Wu, R. Peng and C. Xia, *J. Power Sources*, 2009, **194**, 263.
39 R. Peng, T. Wu, W. Liu, X. Liu and G. Meng, *J. Mater. Chem.*, 2010, **20**, 6218.
40 A. Ringuedé and J. Fouletier, *Solid State Ionics*, 2001, **139**, 167.